



# Design and synthesis of novel thiourea metal complexes with controllable antibacterial properties

Sajjad Rakhshani<sup>1</sup> | Ali Reza Rezvani<sup>1</sup> | Michal Dušek<sup>2</sup> | Václav Eigner<sup>2</sup>

<sup>1</sup>Department of Chemistry, University of Sistan and Baluchestan, PO Box 98135-674, Zahedan, Iran

<sup>2</sup>Institute of Physics, Academy of Sciences of the Czech Republic, Na Slovance 2, 182 21 Praha 8, Czech Republic

## Correspondence

Ali Reza Rezvani, Department of Chemistry, University of Sistan and Baluchestan, PO Box 98135-674, Zahedan, Iran.

Email: ali.reza\_rezvani@yahoo.com

## Funding information

Czech Science Foundation, Grant/Award Number: 15-12719S; University of Sistan and Baluchestan

A new bidentate O,S donor thiourea ligand ( $L^1$ ), namely *N*-(2-hydroxyethyl)-*N'*-2-chlorobenzoylthiourea, and its oxazolidine derivative ( $L^2$ ) were synthesized. Derivative  $L^2$  was used for the preparation of  $Ni(L^2)_2$  and  $Cu(L^2)_2$  complexes. The compounds were investigated using X-ray crystallography and Fourier transform infrared,  $^1H$  NMR and UV-visible spectroscopies. Single-crystal X-ray analysis showed strong hydrogen bonding interactions between carbonyl oxygen and N(10)–H in the  $L^1$  ligand. In addition, the antibacterial activities of these compounds were evaluated against Gram-positive and Gram-negative bacteria, measured using the colony count method. The  $Cu(L^2)_2$  complex exhibited a significant antibacterial activity while the activity of the other compounds was much lower. Finally, the relationship between the structure and antibacterial properties of these compounds was investigated using highest occupied and lowest unoccupied molecular orbital energies calculated by density functional theory method based on the 6-31G\*/LANL2DZ basis set.

## KEYWORDS

bacteria inactivation, colony count method, DFT, hydrogen bond, oxazolidine derivative

## 1 | INTRODUCTION

*N*-Benzoylthiourea and its derivatives are versatile ligands capable of coordinating a range of metal centres. The oxygen, nitrogen and sulfur donors of these ligands provide monobasic bidentate (O,S), neutral monodentate (S) and neutral bidentate (O,N) binding modes.<sup>[1–4]</sup> Thiourea derivatives and their metal complexes exhibit a vast range of biological activities including antitumour,<sup>[5,6]</sup> antitubercular,<sup>[7,8]</sup> insecticidal, antiprotozoal and herbicide activities and they also act as inhibitors for prevention of corrosion of a wide range of metals in various corrosion environments.<sup>[9–11]</sup> Moreover, these compounds have been extensively used as antibacterial agents, which is important in light of a rapid increase of bacterial resistance against known drugs.<sup>[12]</sup>

One of the approaches for increasing the efficacy of antibacterial agents consists of improving their activity

through changing the geometry of the complexes, type of metal ions, oxidation state of metals and total charges on complex ions.<sup>[13]</sup> In this respect, the kinetically labile, square-planar divalent (Cu, Ni and Pd) and octahedral trivalent (Fe, Co and Cr) complexes displayed more activity than other inert complexes, even at low concentrations.<sup>[14]</sup> For instance, the chelation of benzoylthiourea derivatives to metal ions resulted in a significant increase in their biological activities.<sup>[15]</sup> In this respect, weak interactions are also important, especially intramolecular and intermolecular hydrogen bonds. In the case of benzoylthiourea derivatives, there are prominent intramolecular hydrogen bonds between N–H and carbonyl moieties,<sup>[16]</sup> which can influence the coordination modes of *N*-benzoyl-*N'*-substituted thiourea compounds and result in coordination through the sulfur atom of the ligand.<sup>[17]</sup> Therefore, it is possible to influence the biological properties of these compounds by elimination of the

intramolecular hydrogen bonds causing chelation of ligand to metal ion through sulfur and oxygen atoms.

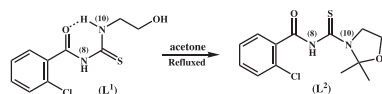
In this article, we report on a new thiourea ligand, *N*-(2-hydroxyethyl)-*N'*-2-chlorobenzoylthiourea ( $L^1$ ). We applied the above-mentioned hydrogen bond elimination by preparing the oxazolidine derivative ( $L^2$ ) of  $L^1$  with a different coordination mode (Scheme 1), and finally we prepared Ni and Cu complexes of  $L^2$ . The compounds were characterized using X-ray crystallography and Fourier transform infrared (FT-IR),  $^1\text{H}$  NMR and UV-visible spectroscopies, and their antibacterial activity was evaluated against standard bacteria using the colony count method. We also considered density functional theory (DFT) results for the highest occupied molecular orbital (HOMO) and lowest unoccupied molecular orbital (LUMO) energies using the 6-31G\*/LANL2DZ basis set for investigation of the relationship between the structures of these compounds and their antimicrobial activities.

## 2 | EXPERIMENTAL

### 2.1 | Methods and Materials

FT-IR spectra were recorded with KBr pellets using a PerkinElmer 781 spectrophotometer. A Bruker 300 MHz AVANCE III spectrometer was utilized to obtain NMR spectra in  $\text{CDCl}_3$  solvent. Melting points were measured with an Electrothermal 9100 apparatus. UV-visible spectra were obtained using a JASCO-570 spectrophotometer. The spectra were measured in dichloromethane solution at room temperature. Single-crystal X-ray data were collected with a SuperNova diffractometer (Rigaku Oxford Diffraction) using mirror-collimated  $\text{Cu K}\alpha$  radiation from a micro-focus sealed X-ray tube and CCD detector (Atlas S2) at 95 K and with a Gemini diffractometer (Rigaku Oxford Diffraction) using graphite-monochromated  $\text{Mo K}\alpha$  radiation from a sealed X-ray tube and CCD detector (Atlas S2) at 120 K. To visualize compound structures, Diamond 3.2 K was used.

All solvents and chemical materials were of reagent grade and were purchased from Merck, including 2-chlorobenzoyl chloride, ammonium thiocyanate, 2-aminoethanol,  $\text{Ni}(\text{CH}_3\text{COO})_2 \cdot 4\text{H}_2\text{O}$ ,  $\text{Cu}(\text{CH}_3\text{COO})_2 \cdot \text{H}_2\text{O}$  and acetone.



**SCHEME 1** Chemical structures of thiourea ligand ( $L^1$ ) and its oxazolidine derivative ( $L^2$ )

## 2.2 | Syntheses

### 2.2.1 | Synthesis of ligand $L^1$

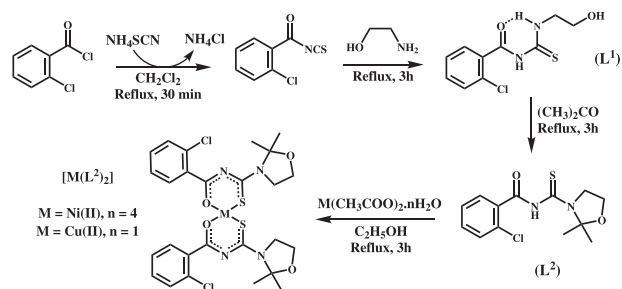
Ligand  $L^1$  was synthesized according to Scheme 2. An amount of 10 mmol of ammonium thiocyanate was dissolved in dichloromethane, and 10 mmol of 2-chlorobenzoyl chloride was added to this solution in a dropwise fashion. The mixture was refluxed for 30 min. After that 10 mmol of 2-aminoethanol was added dropwise to the crude 2-chlorobenzoyl isothiocyanate. Once again the solution was heated to reflux for 3 h. Upon completion of heating, the product was recrystallized from  $\text{CH}_2\text{Cl}_2$ - $\text{C}_2\text{H}_5\text{OH}$ , resulting in a white precipitate which was filtered off. Diffusion of ether into a *N,N*-dimethylformamide (DMF) solution of the ligand gave colourless crystals. Yield 90%; m.p. 121–122 °C. Selected FT-IR data ( $\nu$ ,  $\text{cm}^{-1}$ ): 3525 (O–H), 3252 (N–H), 3051 (Ph–H), 2937 (C–H), 1675 (C–O), 1291 (C–S).  $^1\text{H}$  NMR ( $\text{CDCl}_3$ ;  $\delta$ , ppm): 10.83 (s, 1H, N(8)–H), 9.17 (s, 1H, N(10)–H), 7.29–7.76 (m, 4H, Ph), 3.95–4.03 (m, 4H, – $\text{CH}_2$ ), 1.91–1.94 (t, 1H, OH).

### 2.2.2 | Synthesis of *N*-(2,2-dimethyloxazolidine)-*N'*-2-chlorobenzoylthiourea ligand ( $L^2$ )

The oxazolidine derivative ( $L^2$ ) of the thiourea ligand was synthesized following a procedure as given in the literature.<sup>[18–20]</sup> A mixture of 10 mmol of  $L^1$  and 20 ml of acetone was refluxed for 3 h (Schemes 1 and 2). The product was recrystallized from dichloromethane and identified using FT-IR and  $^1\text{H}$  NMR spectra. Yield 97%; m.p. 143–144 °C. Selected FT-IR data ( $\nu$ ,  $\text{cm}^{-1}$ ): 3241 (N–H), 3051 (Ph–H), 2985 (C–H), 1706 (C–O), 1417 (C–S), 826 (C–Cl).  $^1\text{H}$  NMR ( $\text{CDCl}_3$ ;  $\delta$ , ppm): 8.304 (s, 1H, N(8)–H), 7.29–7.74 (m, 4H, Ph), 4.04–4.13 (m, 4H, – $\text{CH}_2$ ), 1.95 (s, 6H, – $\text{CH}_3$ ).

### 2.2.3 | Synthesis of $\text{Ni}(L^2)_2$ complex

The desired complex was prepared by addition of an ethanolic solution of nickel acetate to a solution of ligand



**SCHEME 2** Synthetic route to ligand  $L^2$  and its Ni(II) and Cu(II) complexes

$L^2$  in a molar ratio of 1:2 at room temperature. The resulting mixture was refluxed for 3 h. The purple precipitate of the complex was filtered and recrystallized from DMF. Yield 90%. Selected FT-IR data ( $\nu$ ,  $\text{cm}^{-1}$ ): 3048 (Ph-H), 2932 (C-H), 1519 (C-O), 1255 (C-S).  $^1\text{H}$  NMR ( $\text{CDCl}_3$ ;  $\delta$ , ppm): 7.25–7.55 (m, 8H, Ph), 3.84–4.06 (m, 8H, 4 $\text{CH}_2$ ), 1.65 (s, 12H,  $-\text{CH}_3$ ).

### 2.2.4 | Synthesis of $\text{Cu}(L^2)_2$ complex

A similar procedure was carried out using  $L^2$  (2 mmol) and  $\text{Cu}(\text{CH}_3\text{COO})_2 \cdot \text{H}_2\text{O}$  (1 mmol) and refluxing for 3 h. The green precipitate was filtered and recrystallized from ethanol. Yield 80%. Selected FT-IR data ( $\nu$ ,  $\text{cm}^{-1}$ ): 3048 (Ph-H), 2932 (C-H), 1514 (C-O), 1249 (C-S).

### 2.3 | X-ray Crystallographic Analysis

The measurements of  $L^1$  and  $\text{Cu}(L^2)_2$  were performed with a Gemini diffractometer and those of  $\text{Ni}(L^2)_2$  were performed with a SuperNova diffractometer, as described in Section 1.1. The data reduction and absorption correction were done with CrysAlis PRO software.<sup>[20]</sup> The structures were solved using charge flipping methods and refined using Jana2006.<sup>[21,22]</sup> The residual electron density maps were visualized using MCE.<sup>[23]</sup> All hydrogen atoms were discernible in difference Fourier maps and could be refined to reasonable geometry. According to common practice, H atoms bonded to C atoms were kept in ideal positions with C-H = 0.96 Å while positions of H atoms bonded to N and O atoms were refined with restrained bond lengths. In both cases  $U_{\text{iso}}(\text{H})$  was set to  $1.2U_{\text{eq}}(\text{C}, \text{N}, \text{O})$ . All non-hydrogen atoms were refined using harmonic refinement. The disordered part of heterocycle in  $\text{Cu}(L^2)_2$  was refined with restrained bond lengths and angles. The overall occupancy was constrained to full with final occupancy ratio of 74:26.

### 2.4 | In Vitro Antimicrobial Studies

According to the literature, the antibacterial properties of the synthesized compounds were measured using bacteria as per the colony count method.<sup>[24–27]</sup> In order to measure the rate of bacterial growth, the bacterial strains were grown in nutrient broth medium supplemented with suspensions of ligand  $L^2$ , or  $\text{Ni}^{2+}$  or  $\text{Cu}^{2+}$  metal complexes at a concentration of 20 ppm. These samples were added into 10 ml of nutrient broth medium to which was added 200  $\mu\text{l}$  of bacteria at a concentration of  $1.5 \times 10^5$  CFU. Blank samples were prepared by growth of the culture in ligand- and metal complex-free media under the same conditions. Then these samples were agitated with a shaker platform at a speed of 200 rpm. After that, 100  $\mu\text{l}$

of each bacterial suspension was dispersed on nutrient agar medium, and finally, the number of colony forming units was enumerated with consideration to the dilution factor after 24 h of incubation at 37 °C.

### 2.5 | Calculation Details

The total computations were accomplished using the DFT (B3LYP) method at the 6-31G\*/LANL2DZ basis set level using the Gaussian 03 program. After optimization, some DFT results for the HOMO and LUMO energies were considered by using the 6-31G\* basis set for C, H, N, O, S and Cl and LANL2DZ for Ni and Cu atoms for investigation of antibacterial properties of the title compounds.

## 3 | RESULTS AND DISCUSSION

### 3.1 | Synthesis and Structural Analysis

According to Scheme 2, the reaction between 2-chlorobenzoyl chloride and ammonium thiocyanate in  $\text{CH}_2\text{Cl}_2$  produced 2-chlorobenzoyl isothiocyanate, and condensation of this compound with 2-aminoethanol resulted in ligand  $L^1$ . This ligand was purified and recrystallized by ether diffusion into a DMF solution of the ligand.

Interestingly, ligand  $L^1$  cannot coordinate metal ions ( $\text{Ni}(\text{II})$  and  $\text{Cu}(\text{II})$ ) in a bidentate manner because the intramolecular hydrogen bond between  $\text{N}(10)\text{-H}$  and carbonyl moiety forces this ligand into a monodentate coordination by keeping the carbonyl oxygen in the *trans* position with respect to sulfur. In order to eliminate this hydrogen bond, we converted  $L^1$  to its oxazolidine derivative  $L^2$  according to Scheme 1.<sup>[28,29]</sup> Ligand  $L^2$  was recrystallized from  $\text{CH}_2\text{Cl}_2$ . The complexes  $\text{Ni}(L^2)_2$  and  $\text{Cu}(L^2)_2$  were prepared by adding a hot ethanolic solution of the respective metal acetate to a solution of  $L^2$  in a molar ratio of 1:2 (Scheme 2). Recrystallization of the complexes from DMF and ethanol yielded suitable crystals for X-ray crystallography. The synthesized  $\text{Ni}(\text{II})$  and  $\text{Cu}(\text{II})$  complexes are soluble in DMF, dimethylsulfoxide,  $\text{CH}_2\text{Cl}_2$  and toluene, and are relatively soluble in water at room temperature. These compounds were characterized using  $^1\text{H}$  NMR, UV and FT-IR spectroscopies and single-crystal X-ray diffraction analysis.

### 3.2 | Spectroscopic Analysis

#### 3.2.1 | FT-IR spectral studies

According to the FT-IR spectrum of ligand  $L^1$ , the band at  $3525 \text{ cm}^{-1}$  should be attributed to the stretching of the O-H group. The medium broad peak at  $3252 \text{ cm}^{-1}$

corresponds to the stretching vibration of N–H groups. Stretching vibrations of C–O and C–S bonds are observed at 1676 and 1291  $\text{cm}^{-1}$ , respectively.<sup>[30]</sup> Symmetric and asymmetric stretching vibrations of ( $-\text{CH}_2$ )

appeared at 2892–2937  $\text{cm}^{-1}$ . The absence of the  $\nu(\text{S}-\text{H})$  band at about 2570  $\text{cm}^{-1}$  and the presence of the  $\nu(\text{N}-\text{H})$  band at about 3252  $\text{cm}^{-1}$  can be explained by formation of the thione tautomer ( $\text{L}^1$ ) in the solid state.

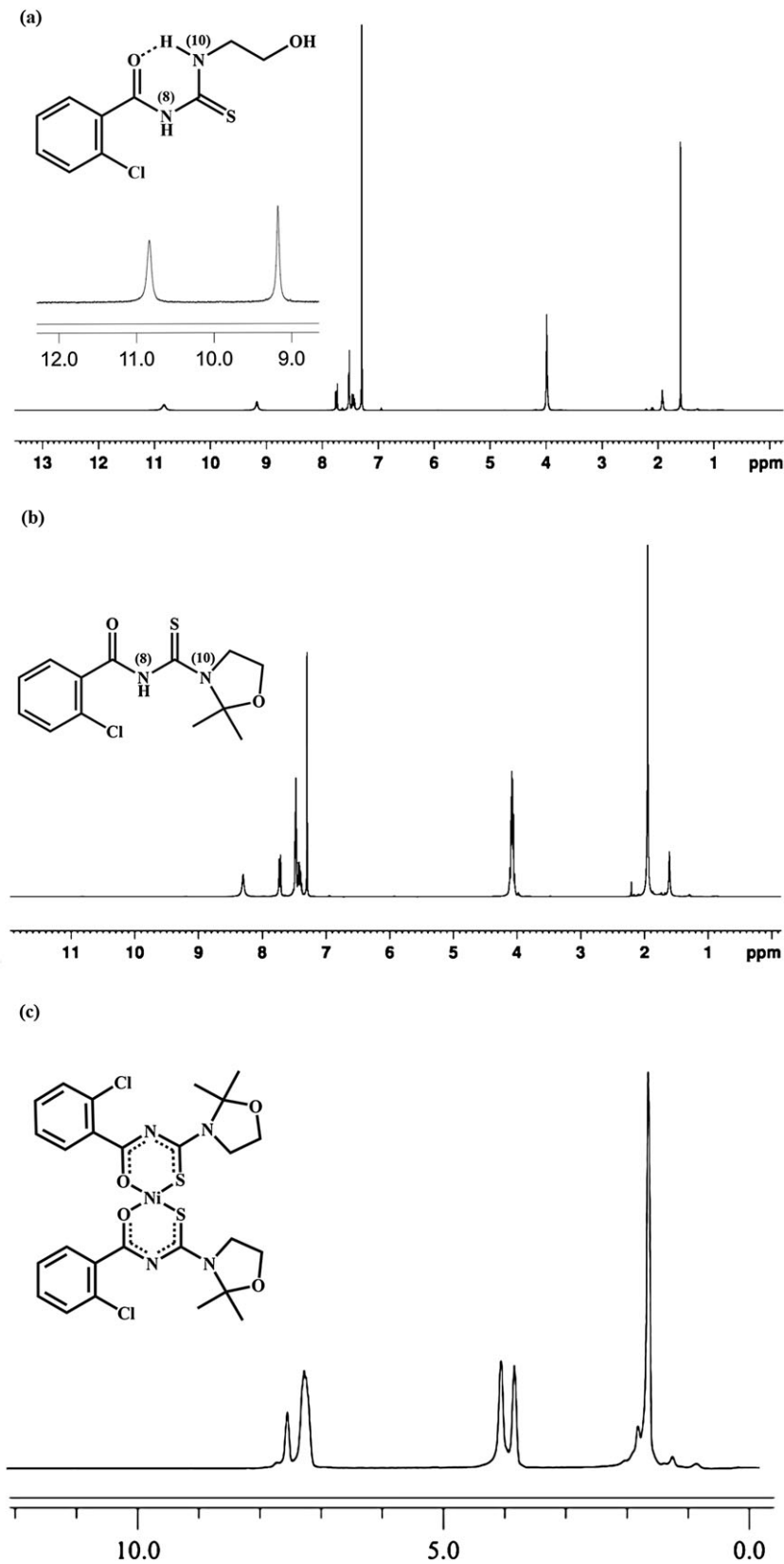


**FIGURE 1**  $^1\text{H}$  NMR spectra of (a)  $\text{L}^1$ , (b)  $\text{L}^2$  and (c)  $\text{Ni}(\text{L}^2)_2$  in  $\text{CDCl}_3$  at room temperature

For  $L^2$ , the main bands at 3241, 1706 and 1417  $\text{cm}^{-1}$  are ascribed to the stretching frequencies of the N(8)–H, C–O and C–S groups. On the other hand, the loss of N(10)–H and OH vibrational frequencies after conversion of  $L^1$  to its oxazolidine derivative  $L^2$  confirmed the formation of the oxazolidine heterocycle.<sup>[18,19]</sup>

After coordination of ligand  $L^2$  to the metal ions, the N(8)–H stretching vibrations disappeared, indicating the loss of H bonded to the N atom of amide group. Also the vibrational frequencies corresponding to C–O and C–S groups in the free ligand were shifted towards lower wavenumber upon complexation, confirming that  $L^2$  is coordinated to  $\text{Ni}^{2+}$  and  $\text{Cu}^{2+}$  through the sulfur and oxygen atoms.<sup>[28,29,31]</sup>

### 3.2.2 | NMR spectral studies

The  $^1\text{H}$  NMR spectra were recorded in  $\text{CDCl}_3$  at room temperature at 300 MHz for ligands and at 250 MHz for the Ni(II) complex. The presence of NH resonances and absence of SH resonances revealed that the thione tautomer instead of thiol tautomer was formed for both  $L^1$   $L^2$ . The  $^1\text{H}$  NMR spectrum of  $L^1$  shows the N(10)–H and N(8)–H resonances at 9.17 and 10.83 ppm. The signal at 1.92 ppm and multiplets at 7.29–7.76 ppm are assigned, respectively, to the OH and phenyl protons in the ligand (Figure 1a).

The same results were obtained for  $L^2$  except the differences caused by the missing N(10)–H and O–H bonds due to the formation of the heterocyclic ring. Therefore, the spectrum of metal-free  $L^2$  exhibits four well-resolved signals at room temperature, N(8)–H, Ph–H,  $-\text{CH}_2$  and  $-\text{CH}_3$  resonances appearing at 8.30, 7.29–7.74, 4.04–4.13 and 1.95 ppm, respectively (Figure 1b).

According to Figure 1(c), the deprotonation of  $L^2$  after complexation to Ni(II) is corroborated by the loss of the N(8)–H signal at 8.30 ppm. In the spectrum of  $\text{Ni}(L^2)_2$ , each peak is shifted downfield from its normal peak position corresponding to  $L^2$ . The diastereotopic hydrogens of  $-\text{CH}_2$  moieties at 4.04–4.13 ppm for  $L^2$  are shifted downfield to 3.84–4.05 ppm for  $\text{Ni}(L^2)_2$  due to the negative induction effect. Similarly, the characteristic signal of the methyl ( $-\text{CH}_3$ ) protons on oxazolidine ring at 1.95 ppm for  $L^2$  is shifted downfield to 1.65 ppm for  $\text{Ni}(L^2)_2$  (Figure 1c). Both FT-IR and NMR data are in agreement with the proposed structures.

### 3.2.3 | UV-visible spectral studies

$\text{CH}_2\text{Cl}_2$  solutions of thiourea ligand  $L^2$  and its Ni(II) and Cu(II) complexes were prepared and the electronic

absorption spectra were recorded in the range 200–800 nm. For  $L^2$ , the absorption bands observed at 230, 285 and 350 nm were assigned to intra-ligand charge transfer transitions  $\pi-\pi^*$  (phenyl ring) and  $n-\pi^*$  (corresponding to C–O and C–S).<sup>[30]</sup>

After coordination of metal ions to ligand  $L^2$ , the absorption bands corresponding to the  $n-\pi^*$  transitions of C–O and C–S display a blue and red shift by 4–10 nm relative to the free ligand.<sup>[32]</sup> In the spectra of metal complexes  $\text{Ni}(L^2)_2$  and  $\text{Cu}(L^2)_2$ , the bands corresponding to the  $n-\pi^*$  transitions of C–O appear at 269 and 275 nm, respectively, thus indicating a hypsochromic shift. On the other hand, the bands at 358 and 360 nm corresponding to the  $n-\pi^*$  transitions of C–S indicate a bathochromic shift due to the complexation of a thione sulfur atom to the metal centre. The band at about 295 nm for the  $\text{Ni}(L^2)_2$  complex is related to ligand-to-metal charge transfer.<sup>[33]</sup> Absorption bands in the visible region, 503 and 586 nm for  $\text{Ni}(L^2)_2$  and  $\text{Cu}(L^2)_2$ , respectively, are due to d–d transitions (Figure 2).<sup>[34–39]</sup>

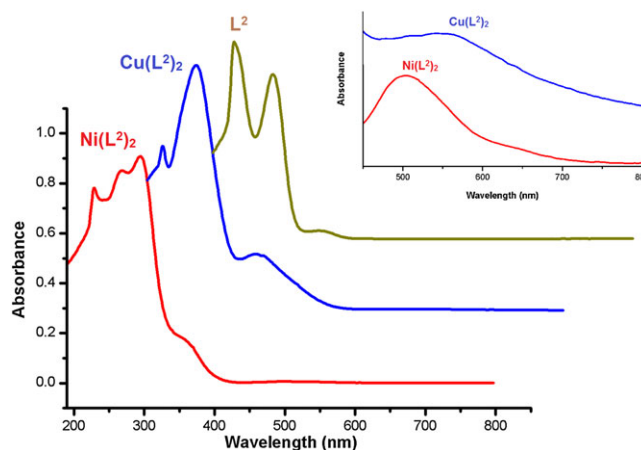


**FIGURE 2** Electronic spectra of ligand  $L^2$  and its Ni(II) and Cu(II) complexes in dichloromethane

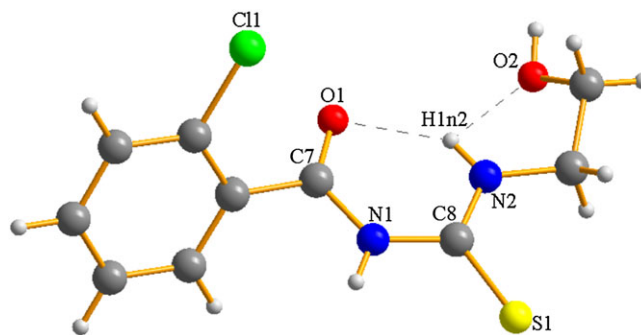


**FIGURE 3** Molecular structure and intramolecular hydrogen bonding of ligand  $L^1$

### 3.3 | Description of Crystal Structures

The structures of  $L^1$  and the Ni(II) and Cu(II) complexes of its oxazolidine derivative were studied using single-crystal X-ray diffraction. Figures 3–5 show the features of their atomic structures. Experimental details of data collection and structure refinement are given in Table 1. Selected bond lengths and bond angles are summarized in Table 2.

#### 3.3.1 | Crystal structure of $L^1$

According to Table 2, the bond length of carbonyl ( $C7-O1 = 1.221(6)$  Å) group of  $L^1$  corresponds to a double bond, while the thiocarbonyl ( $C8-S1 = 1.681(3)$  Å) bond length lies between those of a single and a double bond.<sup>[40]</sup> The C–N bonds,  $C7-N1 = 1.367(7)$  Å,  $C8-N1 = 1.393(2)$  Å,  $C8-N2 = 1.315(8)$  Å, are shorter than the typical single C–N bond length of 1.479 Å due

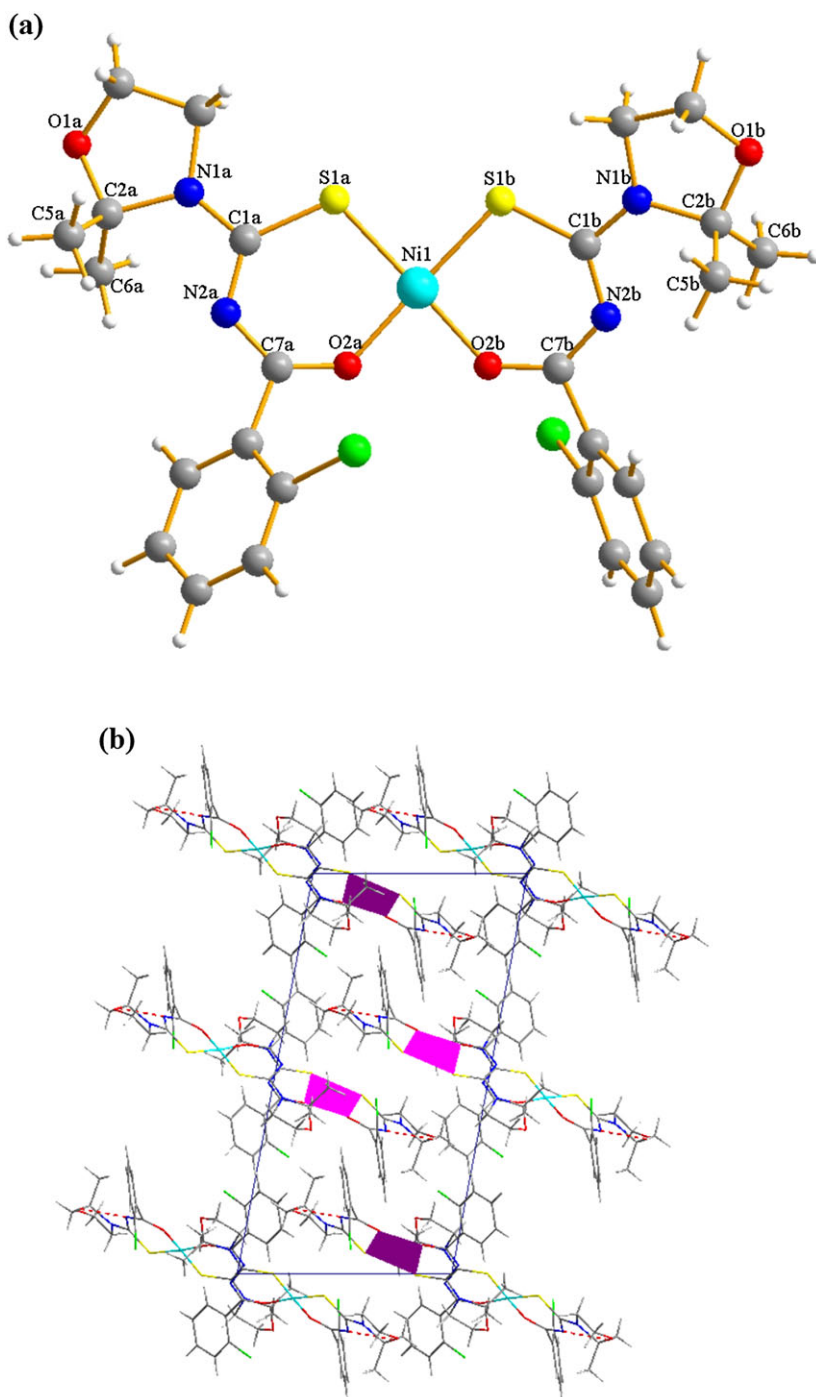


**FIGURE 4** (a) Molecular structure of  $Ni(L^2)_2$  and (b) view of unit cell of  $Ni(L^2)_2$  along the  $b$ -axis

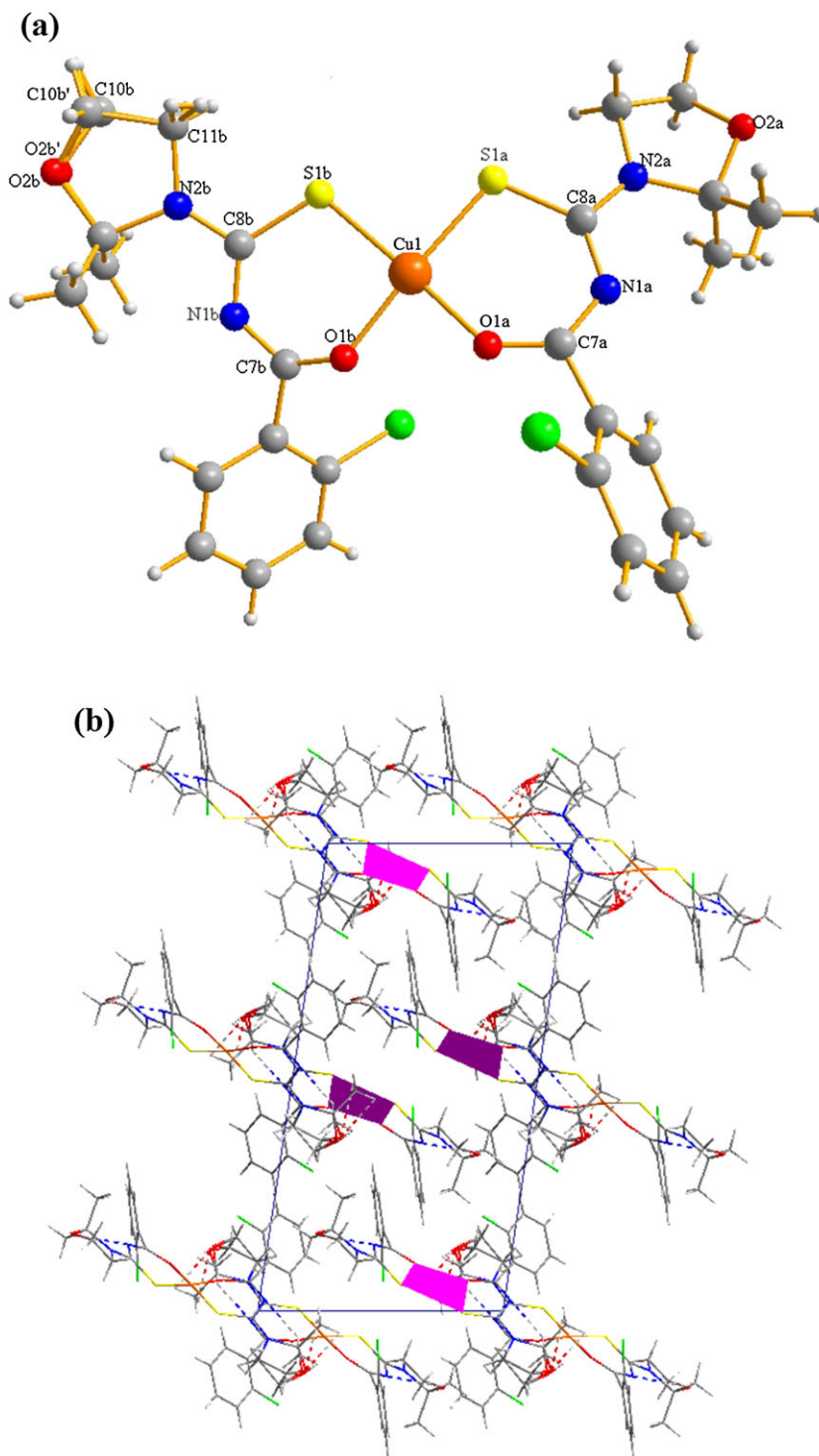


**FIGURE 5** (a) Molecular structure of  $\text{Cu}(\text{L}^2)_2$  and (b) view of unit cell of  $\text{Cu}(\text{L}^2)_2$  along the  $b$ -axis

to the delocalization in the ligand.<sup>[10,19]</sup> This delocalization is also confirmed by values of the angles  $\text{C7-N1-C8} = 127.22(1)^\circ$  and  $\text{C8-N2-C9} = 123.00(9)^\circ$  indicating  $\text{sp}^2$  hybridization on the N1 and N2 atoms.<sup>[20]</sup> The conformation of  $\text{L}^1$  with regard to the thiocarbonyl and carbonyl moieties is twisted, as reflected by the torsion angles  $\text{O1-C7-N1-C8} = 4.520(7)^\circ$ ,  $\text{C7-N1-C8-}$

$\text{N2} = -1.106(2)^\circ$  and  $\text{S1-C8-N1-C7} = 177.022(0)^\circ$ . The C–O and C–S moieties are located at opposite sides of the molecule.

As evident from Figure 3 and Table 2, the N2 atom participates in a bifurcated intramolecular hydrogen bond to carbonyl oxygen (O1) and hydroxyl oxygen (O2). The strong  $1.966(2) \text{ \AA}$  hydrogen bond towards O1 closes the

**TABLE 1** Summary of X-ray diffraction data

	$L^1$	$Ni(L^2)_2$	$Cu(L^2)_2$
Empirical formula	$C_{10}H_{11}Cl_1N_2O_2S_1$	$C_{26}H_{28}Cl_2N_4Ni_1O_4S_2$	$C_{26}H_{28}Cl_2Cu_1N_4O_4S_2$
Formula weight	258.7	654.3	659.1
Temperature (K)	120	95	120
Wavelength (Å)	0.71073	1.54184	0.71073
Crystal system	Triclinic	Monoclinic	Monoclinic
Space group	P -1	P 1 2 <sub>1</sub> /c 1	P 1 2 <sub>1</sub> /c 1
<i>a</i> (Å)	4.5487(2)	11.3603(2)	11.2812(3)
<i>b</i> (Å)	10.3397(6)	11.7544(2)	11.7893(2)
<i>c</i> (Å)	12.4969(7)	21.6307(4)	21.6896(6)
$\alpha$ (°)	78.052(5)	90	90
$\beta$ (°)	88.006(4)	100.7293(15)	98.525(2)
$\gamma$ (°)	89.013(5)	90	90
<i>V</i> (Å <sup>3</sup> )	574.64(5)	2837.93(9)	2852.79(12)
<i>Z</i>	2	4	4
<i>D</i> <sub>calc</sub> (g cm <sup>-3</sup> )	1.4953	1.5313	1.5346
$\mu$ (Mo K $\alpha$ )	0.499	4.411	1.138
<i>F</i> (000)	268	1352	1388
$\theta$ range (°)	3.52 to 29.48	3.96 to 74.53	2.43 to 29.43
Reflections collected	6442	20 408	26 710
Independent reflections	2763	5693	7120
<i>R</i> <sub>int</sub>	0.013	0.0278	0.0199
Data/parameters	2763/155	5693/353	7120/360
GOF on <i>F</i> <sup>2</sup>	1.580	1.670	1.36
<i>R</i> <sub>1</sub> [ <i>I</i> > 3 $\sigma$ ( <i>I</i> )]	0.0265	0.0282	0.0259
<i>wR</i> <sub>2</sub> [ <i>I</i> > 3 $\sigma$ ( <i>I</i> )]	0.0853	0.0863	0.0778
<i>R</i> <sub>1</sub> (all data)	0.0299	0.0294	0.0335
<i>wR</i> <sub>2</sub> (all data)	0.0876	0.0875	0.0815
Largest diff. Peak/hole (e Å <sup>-3</sup> )	0.28/−0.22	0.69/−0.31	0.30/−0.27

ring C8–N1–C7–O1–H1n2–N2 into a planar structure, which can compel the monodentate coordination of  $L^1$  to metal ions.<sup>[17]</sup>

### 3.3.2 | Crystal structure of $Ni(L^2)_2$ complex

Figure 4(a) shows that the Ni centre is chelated by two deprotonated ligands coordinated in the bidentate O,S mode in *cis* arrangement, giving rise to a nearly square planar geometry around Ni (O2b–Ni1–Sa1 = 179.29(3)°, O2a–Ni1–S1b = 174.88°, O2a–Ni1–S1a = 94.72°, O2b–Ni1–S1b = 94.79°, Ni1–O2b–C7b–N2b = 3.651°, Ni1–S1b–C1b–N2b = 19.534°).

The carbonyl and thiocarbonyl bond distances changed from average values of 1.2216 and 1.6813 Å for the free ligand to 1.267 and 1.74 Å for the complex (C7a–O2a = 1.26(6) Å, C1a–S1a = 1.74(1) Å; C7b–O2b = 1.26(5) Å, C1b–S1b = 1.73(6) Å). The bond lengths of C–N moieties (C7–N2a = 1.32(2) Å, C1a–N2a = 1.34(6) Å, C1a–N1a = 1.33(5) Å, C7b–N2b = 1.31(9) Å, C1b–N2b = 1.34(6) Å, C1b–N1b = 1.33(3) Å) are shorter than for a typical single C–N bond. This variation in C–O, C–S and C–N bond lengths of the complex indicates a marked electronic delocalization in the chelate rings.

The crystal packing of  $Ni(L^2)_2$  demonstrates a weak intermolecular hydrogen bonding, C6b–H1c6b $\cdots$ N2b<sup>i</sup> (symmetry code: (i) 1 – *x*, –0.5 + *y*, 0.5 – *z*) (Table 2; Figure 4b).

TABLE 2 Selected bond lengths, angles, torsion angles and interactions

$L^1$		$Ni(L^2)_2$		$Cu(L^2)_2$	
Bond lengths (Å)		Bond lengths (Å)		Bond lengths (Å)	
C7–O1	1.221(6)	Ni1–O2b	1.861(9)	Cu1–O1b	1.918(3)
C8–S1	1.681(3)	Ni1–S1b	2.145(3)	Cu1–S1b	2.244(3)
C7–N1	1.367(7)	Ni1–O2a	1.857(1)	Cu1–O1a	1.925(4)
C8–N1	1.393(1)	Ni1–S1a	2.146(7)	Cu1–S1a	2.227(3)
C8–N2	1.315(8)	C7b–O2b	1.265(0)	C7a–O1a	1.258(5)
N2–H1n2	0.680(9)	C1b–S1b	1.736(6)	C8a–S1a	1.735(9)
N1–H1n1	0.859(7)	C7b–N2b	1.319(3)	C7b–O1b	1.262(4)
		C1b–N2b	1.346(7)	C8b–S1b	1.743(0)
		C1b–N1b	1.333(5)	C7a–N1a	1.318(4)
		C7a–O2a	1.266(8)	C8a–N1a	1.350(8)
		C1a–S1a	1.741(7)	C8a–N2a	1.331(1)
		C7a–N2a	1.322(1)	C7b–N1b	1.326(3)
		C1a–N2a	1.346(8)	C8b–N1b	1.342(2)
		C1a–N1a	1.335(6)	C8b–N2b	1.331(8)
Bond angles (°)		Bond angles (°)		Bond angles (°)	
O1–C7–N1	122.97(5)	O2b–Ni1–S1a	176.29(3)	O1a–Cu1–S1b	174.99(0)
S1–C8–N1	119.11(3)	O2a–Ni1–S1b	174.88(3)	O1b–Cu1–S1a	173.19(2)
N1–C8–N2	117.58(2)	O2a–Ni1–S1a	94.72(3)	O1a–Cu1–S1a	92.89(1)
C7–N1–C8	122.22(1)	O2b–Ni1–S1b	94.79(3)	O1b–Cu1–S1b	91.79(3)
C8–N2–C9	123.00(9)				
Torsion angles (°)		Torsion angles (°)		Torsion angles (°)	
O1–C7–N1–C8	4.52(1)	Ni1–O2b–C7b–N2b	3.65(1)	Cu1–S1a–C8a–N1a	−16.13(6)
C7–N1–C8–N2	−1.10(6)	Ni1–S1b–C1b–N2b	19.54(3)	Cu1–O1a–C7a–N1a	4.68(6)
S1–C8–N1–C7	177.02(2)	Ni1–O2b–C7a–N2a	27.75(5)	Cu1–S1b–C8b–N1b	−21.41(7)
		Ni1–S1a–C1a–N2a	18.07(1)	Cu1–O1b–C7b–N1b	−33.99(9)
Hydrogen bond geometries					
Compound	D–H...A	D–H (Å)	H...A (Å)	D...A (Å)	D–H...A (°)
$L^1$	N2–H1n2...O1	0.860(8)	1.966(2)	2.645(3)	134.92(0)
	N2–H1n2...O2	0.860(8)	2.465(9)	2.748(3)	99.92(4)
$Ni(L^2)_2$	C6b–H1c6b...N2b <sup>i</sup>	0.824(6)	2.481(0)	2.996(0)	113.49(1)
$Cu(L^2)_2$	C13b–H1c13b...O1b <sup>ii</sup>	0.960(0)	2.904(3)	3.473(6)	119.08(1)
	C12a–H3c12a...N1b <sup>iii</sup>	0.959(9)	2.888(7)	3.684(2)	140.94(4)
(i) 1 – x, –0.5 + y, 0.5 – z; (ii) 1 – x, 1 – y, –z; (iii) 1 + x, –1 + y, z					

### 3.3.3 | Crystal structure of $Cu(L^2)_2$ complex

The Ni and Cu complexes are isotypic. The Cu complex (Figure 5a) has a similar slightly distorted square planar geometry around the metal atom (O1a–Cu1–S1b = 174.99°, O1b–Cu1–S1a = 173.19°, O1a–Cu1–

S1a = 92.83°, O1b–Cu1–S1b = 92.80°; Cu1–S1a–C8a–N1a = −16.136°, Cu1–O1a–C7a–N1a = 4.686°), and it also features a decrease of the bond order of carbonyl and thiocarbonyl moieties as well as an increase of C–N bond orders. This again indicates the presence of marked delocalization of electron density in the chelate ring of the complex.<sup>[33,34]</sup> Unlike the Ni complex, one of the

oxazolidine ring moieties is disordered with occupancy of the minor disordered part refined to 0.259(4). The atom labels of the minor disordered part are indicated by a prime: O2b', C10b', C11b' and corresponding hydrogen atoms. The main intermolecular interactions are C13b—H1c13b...O1b<sup>i</sup> and C12a—H3c12a...N1b<sup>ii</sup> (symmetry code: (i) 1 - x, 1 - y, -z; (ii) 1 + x, -1 + y, z) (Table 2; Figure 5b).

### 3.4 | Antibacterial Assay

The free ligand ( $L^2$ ) and its  $Ni^{2+}$  and  $Cu^{2+}$  metal complexes were investigated for their antibacterial activity against Gram-negative (*Escherichia coli*; *E. coli* ATCC 25922) and Gram-positive (*Staphylococcus aureus*; *S. aureus* ATCC 25923) bacteria. The studied compounds have varying bactericidal effects on the tested bacterial strains. For both tested bacterial strains, the antibacterial activity of the complexes was better than that of the free ligand, as explained by Tweedy's chelation theory.<sup>[41]</sup> According to this theory, the chelation reaction diminishes the polarity of the metal ions through partial sharing of their positive charge with donor groups and delocalization of electrons over the chelating ring.<sup>[42]</sup> This augments the lipophilic feature of the  $Ni(L^2)_2$  and  $Cu(L^2)_2$

complexes compared with the free ligand and increases their ability to permeate the peptidoglycan layer of cell walls or the lipid layer of cell membranes. While ligand  $L^1$  is unable to coordinate to the metal ions in a bidentate manner due to the strong intramolecular hydrogen bond between N2—H1n2 and the carbonyl oxygen atom (O1) (Figure 3), its oxazolidine derivative  $L^2$  can provide such complexes. As a result, the elimination of the intramolecular hydrogen bond in  $L^2$  leads to the increase of antibacterial properties of complexes.

We found that  $L^2$  and its  $Ni(II)$  and  $Cu(II)$  complexes were more powerful bactericidal agents against the Gram-negative bacterium than against the Gram-positive bacterium. The difference in the efficacy of these agents can be ascribed to the differences in the cell wall structure of the otherwise similar Gram-negative and Gram-positive bacteria; a Gram-negative bacterium has a thin peptidoglycan layer and an outer membrane that contains proteins, phospholipids and lipopolysaccharide, while a Gram-positive bacterium has a thick peptidoglycan layer that contains teichoic and lipoteichoic acid. Therefore, the cell wall of a Gram-negative bacterium is more polar, and the permeation of  $Ni(L^2)_2$  and  $Cu(L^2)_2$  complexes into the microorganism is facilitated by this polarity.<sup>[43]</sup> Therefore, the efficacy of the investigated

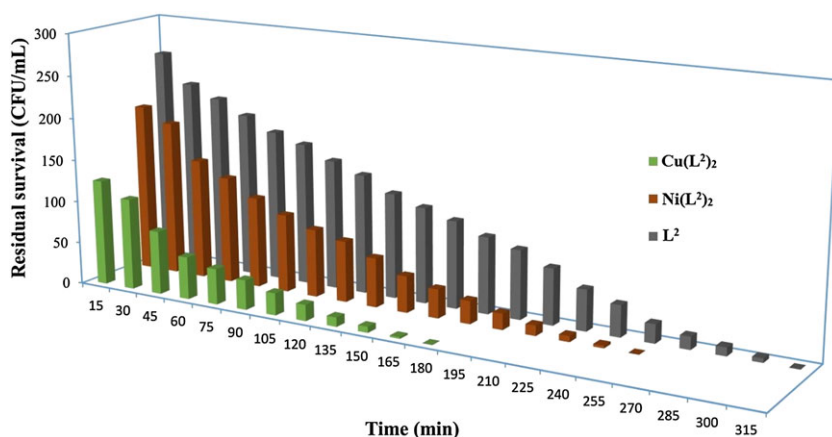


FIGURE 6 Plot of survival of *E. coli* with  $L^2$ ,  $Ni(L^2)_2$  and  $Cu(L^2)_2$

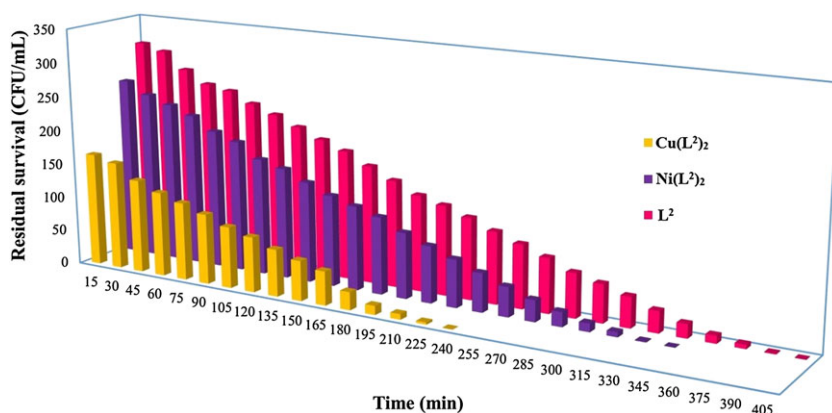
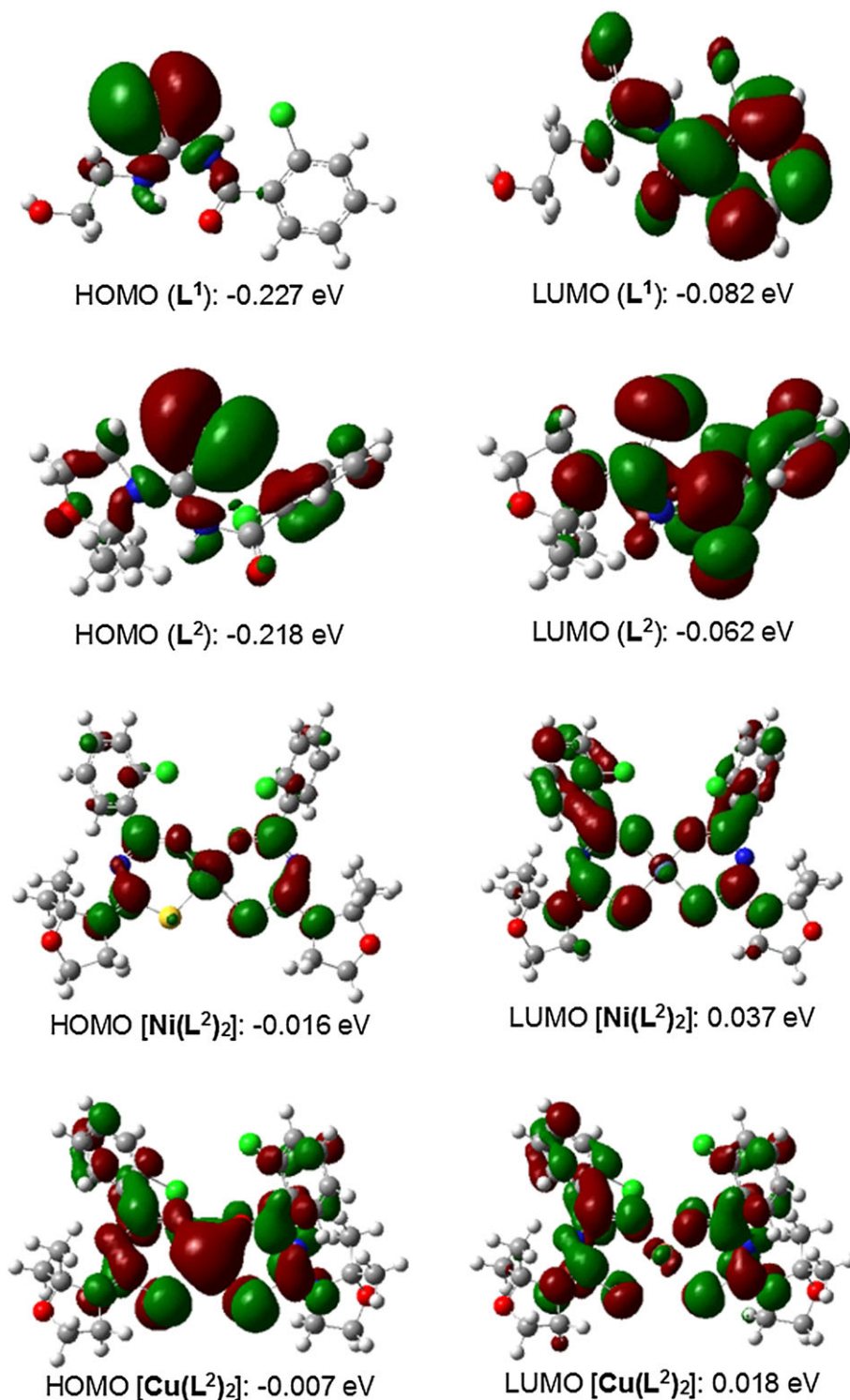


FIGURE 7 Plot of survival of *S. aureus* with  $L^2$ ,  $Ni(L^2)_2$  and  $Cu(L^2)_2$

compounds against *E. coli* is greater than against *S. aureus*.<sup>[25,44,45]</sup>

Furthermore, the strengths of the antibacterial activity are associated with the elongation or shortening of the C—O and C—S bond lengths in the complexes, because the elongation of such bonds increases both the polarity and reactivity of C—O and C—S bonds.<sup>[46]</sup> Pursuant to

the crystallographic data (Table 2), the C—O and C—S bond lengths are larger for Cu(L<sup>2</sup>)<sub>2</sub>, and indeed the antibacterial activity of this complex is greater than that of Ni(L<sup>2</sup>)<sub>2</sub> due to better connection of the carbonyl and the thiocarbonyl to the microorganism.<sup>[47–49]</sup> Thus, Cu(L<sup>2</sup>)<sub>2</sub> is the most efficient inhibitor among the three investigated compounds (Figures 6 and 7).



**FIGURE 8** Frontier molecular orbitals of the studied compounds

### 3.5 | Structure–Activity Relationship

The optimization of the molecular structures of  $L^1$ ,  $L^2$  and Ni(II) and Cu(II) complexes of  $L^2$  was accomplished using the DFT method (B3LYP) at 6-31G\* and LANL2DZ basis set level. After that, DFT results for the frontier molecular orbital energies were obtained. The frontier molecular orbitals of these samples are shown in Figure 8.

These results confirm the inverse connection between the size of the band gap ( $\Delta E_{L-H}$ ) and the antibacterial activities of these samples.<sup>[38,39,50–52]</sup> In other words, the smaller is the difference between LUMO and HOMO energies, the greater is the antibacterial activity. According to Figure 8, the  $Cu(L^2)_2$  complex has the narrowest band gap, which conforms to its greatest antibacterial activity (Figures 6 and 7) among the investigated compounds.

## 4 | CONCLUSIONS

The intramolecular hydrogen bond in ligand  $L^1$  prevents coordination of the carbonyl moiety to metal ions and causes synthesis of a mixture of *cis* and *trans* complexes. To eliminate this intramolecular hydrogen bond and favour a bidentate chelating of ligand to metal ion, we prepared the oxazolidine derivative of the  $L^1$  ligand,  $L^2$ , and used it for synthesis of the bis-chelate Ni(II) and Cu(II) complexes. The crystal structures of  $Ni(L^2)_2$  and  $Cu(L^2)_2$  revealed that the Ni and Cu atoms display a nearly square planar geometry with two bidentate ligands having oxygen and sulfur as donor atoms in *cis* position. *In vitro* antibacterial activity experiments against *E. coli* and *S. aureus* showed that the  $Cu(L^2)_2$  complex has the strongest antibacterial activity among the investigated compounds. This is due to the chelation of  $L^2$  to  $Cu^{2+}$  ion, which decreases its polarity and increases the lipophilic property. Theoretical computations illustrate that the antibacterial properties of the synthesized compounds are related to the difference between frontier orbital energies, where a decrease in the band gap energy corresponds to an increase of the antibacterial activity.

## ACKNOWLEDGEMENTS

We thank USB for financial support. The crystallographic investigation was supported by project 15-12719S of the Czech Science Foundation using instruments of the ASTRA laboratory established within the Operation Program Prague Competitiveness – project CZ.2.16/3.1.00/24510.

## ORCID

Sajjad Rakhshani  <http://orcid.org/0000-0002-0490-3130>

Ali Reza Rezvani  <http://orcid.org/0000-0003-2681-9906>

Václav Eigner  <http://orcid.org/0000-0003-1014-3980>

## REFERENCES

- [1] D. G. Patil, M. R. Chedekel, *J. Org. Chem.* **1984**, *49*, 997.
- [2] Z. F. Li, X. X. Cheng, G. Li, H. J. Lu, H. F. Zhang, *J. Lumin.* **2010**, *130*, 2192.
- [3] N. Selvakumaran, N. S. Weng, E. R. T. Tiekink, R. Karvembu, *Inorg. Chim. Acta* **2011**, *376*, 278.
- [4] A. M. Mansour, *Appl. Organometal. Chem.* **2018**, *32*, e3928.
- [5] W. Schiessl, R. Puchta, Ž. D. Bugarčić, F. W. Heinemann, R. Eldik, *Eur. J. Inorg. Chem.* **2007**, 1390.
- [6] D. C. Schroeder, *Chem. Rev.* **1955**, *55*, 181.
- [7] E. Rodríguez-Fernández, E. García, M. R. Hermosa, A. Jiménez-Sánchez, M. Mar Sánchez, E. Monte, J. J. Criado, *J. Inorg. Biochem.* **1999**, *75*, 181.
- [8] K. Chandrasekhara Pillai, R. Narayan, *J. Electrochem. Soc.* **1978**, *125*, 1393.
- [9] A. Mesbah, S. Jacques, E. Rocca, M. François, J. Steinmetz, *Eur. J. Inorg. Chem.* **2011**, 1315.
- [10] M. Ozcan, I. Dehri, M. Erbil, *Appl. Surf. Sci.* **2004**, *236*, 155.
- [11] K. F. Khaled, *Appl. Surf. Sci.* **2010**, *256*, 6753.
- [12] S. Saha, D. Dhanasekaran, S. Chandraleka, N. Thajuddin, A. Panneerselvam, *Adv. Biol. Res.* **2010**, *4*, 224.
- [13] H. M. Parekh, P. B. Pansuriya, M. N. Patel, *Polish J. Chem.* **2005**, *79*, 1843.
- [14] V. Bobbarala, *A Search for Antibacterial Agents*, InTech, Rijeka, Croatia **2012**.
- [15] B. H. Abdullah, Y. M. Salh, *Orient. J. Chem.* **2010**, *26*, 763.
- [16] G. Kurt, F. Sevgi, B. Mercimek, *Chem. Pap.* **2009**, *63*, 548.
- [17] K. R. Koch, Y. Wang, A. Coetzee, *J. Chem. Soc. Dalton Trans.* **1999**, *63*, 1013.
- [18] E. D. Bergmann, *Chem. Rev.* **1953**, *53*, 309.
- [19] M. Al-Masum, B. W. Lott, N. Ghazialsharif, *Int. J. Org. Chem.* **2012**, 362.
- [20] E. D. Bergmann, E. Zimkin, S. Pinchas, *Recl. Trav. Chim. Pays-Bas* **1952**, *71*, 168.
- [21] Crys AlisPro, *Rigaku Oxford Diffraction*, **2015**.
- [22] L. Palatinus, G. Chapuis, *J. Appl. Crystallogr.* **2007**, *40*, 786.
- [23] V. Petricek, M. Dusek, L. Palatinus, *Z. Kristallogr.* **2014**, *229*, 345.
- [24] J. Rohlicek, M. Husak, *J. Appl. Crystallogr.* **2007**, *40*, 600.
- [25] N. Talebian, S. M. Amininezhad, M. Douidi, *J. Photochem. Photobiol. B* **2013**, *120*, 66.
- [26] S. M. Amininezhad, A. R. Rezvani, M. Amouheidari, S. M. Amininejad, S. Rakhshani, J. Zahedan, *Res. Med. Sci.* **2015**, *17*, e1053.
- [27] H. Naeimi, Z. S. Nazifi, S. M. Amininezhad, *J. Photochem. Photobiol. B* **2015**, *149*, 180.
- [28] S. Bourne, K. R. Koch, *J. Chem. Soc. Dalton Trans.* **1993**, 2071.
- [29] K. R. Koch, C. Sacht, S. Bourne, *Inorg. Chim. Acta* **1995**, *232*, 109.

- [30] M. Atiş, F. Karipcin, B. Sarıboğa, M. Taş, H. Çelik, *Spectrochim. Acta A* **2012**, *98*, 290.
- [31] A. Irving, K. R. Koch, M. Matoetoe, *Inorg. Chim. Acta* **1993**, *206*, 193.
- [32] J. Barret, F. S. Deghaidy, *Spectrochim. Acta A* **1975**, *31*, 707.
- [33] A. Shrivastav, N. K. Singh, S. M. Singh, *BioMetals* **2003**, *16*, 311.
- [34] A. B. P. Lever, *Inorganic Electronic Spectroscopy*, 2nd ed., Elsevier, Amsterdam **1984**.
- [35] M. Mikami, I. Nakagawa, T. Shimanouchi, *Spectrochim. Acta A* **1967**, *23*, 1037.
- [36] M. C. Prabahkara, H. S. Bhojya Naik, *BioMetals* **2008**, *21*, 675.
- [37] M. Hanif, Z. H. Chohan, *Appl. Organometal. Chem.* **2013**, *27*, 36.
- [38] W. Yang, H. Liu, M. Li, F. Wang, W. Zhou, J. Fan, *J. Inorg. Biochem.* **2012**, *116*, 97.
- [39] M. H. Klingele, P. D. W. Boyd, B. Moubaraki, K. S. Murray, S. Brooker, *Eur. J. Inorg. Chem.* **2006**, *573*.
- [40] W. Hernández, E. Spodine, J. C. Muñoz, L. Beyer, U. Schröder, J. Ferreira, M. Pavani, *Bioinorg. Chem. Appl.* **2003**, *1*, 271.
- [41] N. Dharmaraj, *Transition Met. Chem.* **2001**, *26*, 105.
- [42] T. D. Thangadurai, K. Natarajan, *Transition Met. Chem.* **2001**, *26*, 500.
- [43] F. Khosravi, H. Mansouri-Torshizi, *J. Biomol. Struct. Dyn.* **2017**, *35*, 1.
- [44] A. G. Rincón, C. Pulgarin, *Appl. Catal. B* **2004**, *49*, 99.
- [45] A. Pal, S. O. Pehkonen, L. E. Yu, M. B. Ray, *J. Photochem. Photobiol. A* **2007**, *186*, 335.
- [46] J. Xie, Z. Cheng, W. Yang, H. Liu, W. Zhou, M. Li, Y. Xu, *Appl. Organometal. Chem.* **2015**, *29*, 157.
- [47] B. A. Kellogg, L. Garrett, Y. Kovtun, K. C. Lai, B. Leece, M. Miller, G. Payne, R. Steeves, K. R. Whiteman, W. Widdison, *Bioconjugate Chem.* **2011**, *22*, 717.
- [48] H. Dong, T. Hou, Y. Zhao, X. Fu, Y. Li, *Comput. Theor. Chem.* **2012**, *1001*, 51.
- [49] E. Movahedi, A. R. Rezvani, *J. Mol. Struct.* **2017**, *1139*, 407.
- [50] L. Padmaja, C. Ravikumar, D. Sajan, I. H. Joe, V. S. Jayakumar, G. R. Pettit, O. F. Nielsen, *J. Raman Spectrosc.* **2009**, *40*, 419.
- [51] N. Tidjani-Rahmouni, N. E. H. Bensiradj, S. Djebbar, O. Benali-Baitich, *J. Mol. Struct.* **2014**, *1075*, 254.
- [52] U. M. Rafi, D. Mahendiran, A. K. Haleel, R. P. Nankar, M. Doble, A. K. Rahiman, *New J. Chem.* **2016**, *40*, 2451.

## SUPPORTING INFORMATION

Additional Supporting Information may be found online in the supporting information tab for this article.

**How to cite this article:** Rakhshani S, Rezvani AR, Dušek M, Eigner V. Design and synthesis of novel thiourea metal complexes with controllable antibacterial properties. *Appl Organometal Chem.* 2018;e4342. <https://doi.org/10.1002/aoc.4342>